Biomaterials 41 (2015) 151–165

Contents lists available at ScienceDirect

Biomaterials

journal homepage: www.elsevier.com/locate/biomaterials

Microchannel-based regenerative scaffold for chronic peripheral nerve interfacing in amputees

Akhil Srinivasan [a], Mayank Tahilramani [a], John T. Bentley [a], Russell K. Gore [a, b], Daniel C. Millard [a], Vivek J. Mukhatyar [a], Anish Joseph [a], Adel S. Haque [a], Garrett B. Stanley [a], Arthur W. English [c], Ravi V. Bellamkonda [a, *]

[a] Wallace H Coulter Department of Biomedical Engineering, Georgia Institute of Technology and Emory University School of Medicine, Atlanta, GA 30332, USA
[b] Department of Neurology, Emory University School of Medicine, Atlanta, GA 30322, USA
[c] Department of Cell Biology, Emory University School of Medicine, Atlanta, GA 30322, USA

ARTICLE INFO

Article history:
Received 31 July 2014
Accepted 7 November 2014
Available online 9 December 2014

Keywords:
Nerve regeneration
Nerve guide
Polydimethylsiloxane
Peripheral nerve interfacing
Neural interfacing
Microchannel

ABSTRACT

Neurally controlled prosthetics that cosmetically and functionally mimic amputated limbs remain a clinical need because state of the art neural prosthetics only provide a fraction of a natural limb's functionality. Here, we report on the fabrication and capability of polydimethylsiloxane (PDMS) and epoxy-based SU-8 photoresist microchannel scaffolds to serve as viable constructs for peripheral nerve interfacing through *in vitro* and *in vivo* studies in a sciatic nerve amputee model where the nerve lacks distal reinnervation targets. These studies showed microchannels with 100 μm × 100 μm cross-sectional areas support and direct the regeneration/migration of axons, Schwann cells, and fibroblasts through the microchannels with space available for future maturation of the axons. Investigation of the nerve in the distal segment, past the scaffold, showed a high degree of organization, adoption of the microchannel architecture forming 'microchannel fascicles', reformation of endoneurial tubes and axon myelination, and a lack of aberrant and unorganized growth that might be characteristic of neuroma formation. Separate chronic terminal *in vivo* electrophysiology studies utilizing the microchannel scaffolds with permanently integrated microwire electrodes were conducted to evaluate interfacing capabilities. In all devices a variety of spontaneous, sensory evoked and electrically evoked single and multi-unit action potentials were recorded after five months of implantation. Together, these findings suggest that microchannel scaffolds are well suited for chronic implantation and peripheral nerve interfacing to promote organized nerve regeneration that lends itself well to stable interfaces. Thus this study establishes the basis for the advanced fabrication of large-electrode count, wireless microchannel devices that are an important step towards highly functional, bi-directional peripheral nerve interfaces.

1. Introduction

Prosthetics aim to restore the functional capacity once held by an amputee. A number of neural prostheses have been developed with the goal to artificially substitute or mimic sensorimotor functions in patients. For instance, this goal can be accomplished via an interface with the peripheral nervous system by means of implanted electrodes capable of neuromuscular stimulation and neural signal recording. Stable bi-directional communication could allow for a natural control over advanced prosthetic limbs and other similar assistive devices for amputees.

State of the art peripheral nerve interfacing has centered around three main types of device designs: cuff, penetrating, and regenerative sieve electrodes. Cuff and penetrating interfaces face a large tradeoff between the ability to selectively interface with individual axons versus the amount of disruption to the nerve and long-term stability as a result of trying to get in close proximity to axons [1]. Cuff electrodes, which wrap around the nerve, cause minimal damage and provide long-term stability at the expense of stimulation/recording specificity due to a lack of direct contact with

* Corresponding author. Wallace H Coulter Department of Biomedical Engineering, Georgia Institute of Technology and Emory University School of Medicine, 313 Ferst Drive, Atlanta, GA 30332, USA. Tel.: +1 404 385 5038; fax: +1 404 385 5044.
E-mail addresses: ravi@gatech.edu, bellamkonda@emory.edu (R.V. Bellamkonda).

http://dx.doi.org/10.1016/j.biomaterials.2014.11.035
0142-9612/

individual axons [1–4]. In contrast the Utah Slanted Electrode Array (USEA) penetrates the nerve and provides enhanced specificity through direct contact between the electrodes and axons. However, the insertion causes injury and the electrodes elicit chronic inflammation and scar tissue [5]. An alternative to combat these negative outcomes is a regenerative approach, where transected axons grow into specific geometries within close proximity of electrodes [6]. The hallmark Sieve Electrode is implanted so axons are forced to regenerate through its many perforations/holes making contact with ring electrodes [7]. However, this design has few viable electrodes because the extracellular potential of an axon's action potential (AP) is small. Furthermore, there is a spatial dependence of the electrodes to the nodes of Ranvier, which occur at least every 2 mm and are where the extracellular potential is largest [1,8–10].

Microchannels offer a unique opportunity to take advantage of the regenerative approach while circumventing issues with small APs and the node of Ranvier dependence, as detailed elsewhere [2,9,11–13]. Briefly, if a nerve regenerates through electrically insulating microchannels, small groups of axons can be isolated from each other and the surrounding low impedance extracellular fluid. Limiting the extracellular volume increases the extracellular resistance and from Ohm's law, increases the extracellular potential of an axon's AP [2]. Using microchannels with a length of 3 mm ensures a node of Ranvier will always be contained within the microchannels making them spatially independent of the nodes. Such conditions have been validated *in vitro*. APs from axons were recorded from inside a microchannel, the spatial position of the axons changed, and recordings taken again without any significant difference in AP signal amplitude [9].

However, the underlying success of a regenerative microchannel interface as a dependable solution for neural interfacing is not only its ability to detect high quality APs, but also a function of long term tolerance by the peripheral nervous system. Thus, the neural implant is inherently dependent on the chronic condition of the matured nerve post-regeneration. To prevent neuropathic complications post-implantation, the device must facilitate sufficient room for nerve maturation over time while in close contact with as many axons as possible to obtain clear neural signals. The device must also facilitate healthy nerve characteristics such as a maintained tissue architecture, established myelinated fibers, and prominent axon profiles through the regeneration and maturation phases [7,14,15]. Lacking such nerve characteristics has proven to yield poor nerve functionality, compressive axonopathy, and neuromas which result in poor translation of neural signal and loss of nerve utility [7,15–19]. The tendency of regenerating injured nerves to form neuromas is also a major clinical concern for amputees due to associated chronic pain as well as a major concern for specificity during neural interfacing due to characteristic random AP firing [20–24]. Neuromas not only negatively impact performance but also the tolerance of an implant by the host's PNS by creating a hostile environment not conducive to typical axon regeneration and maturation. They are abnormal in their physiological characteristics as manifested by a marked degeneration and absence of myelination and axons, myelin debris, a decrease in Schwann cell population, loss of nerve organization/structure and oriented axon growth, loose basal lamina structure surrounding axons, edema and swelling, and the overall decline of axonal health in a regenerating nerve [17,18,21–23,25]. If a regenerative microchannel interface is unable to support the maturation and chronic retention of healthy axons, then even if it can record action potentials, it still fails from a biological perspective due to these neuropathic complications.

Our long term goal is to establish a large-electrode count microchannel interface for bi-directional communication within an amputated nerve. The basic design of the microchannel architecture is inspired by work from Dr. Fawcett and Dr. Lacour while at the University of Cambridge, and is shown in Fig. 1. The interface utilizes top and bottom polydimethylsiloxane (PDMS) layers with SU-8 walls forming series of adjacent microchannels. Prior to implantation, the array of microchannels is rolled onto itself forming the device filled with microchannel conduits, mimicking the general cross-sectional architecture of a nerve. The device is implanted so that the transected axons can regenerate through the microchannels and over the electrodes housed in the bottom PDMS layer for interfacing.

Here, we focus on the response of the regenerating nerve to an artificially imposed microchannel obstacle and separately the ability to obtain neural signals from these microchannels that are meaningful for the eventual goal of neural interfacing. We first validate cytocompatibility of the scaffolding materials through *in vitro* experimentation. We then explore the capability of axons in an amputated nerve that lacks distal reinnervation targets to regenerate through the device and mature in a PDMS and SU-8 based microchannel scaffolding. Furthermore, we characterize the regenerated nerve from a morphological perspective once the axons have grown out of the microchannel scaffolding and attempt to assess whether neuroma formation is a major concern by evaluating the characteristics described previously common to neuromas. Specifically we consider the presence or lack of organization within the nerve and oriented axon regeneration, Schwann cells and myelin deposition on axons, tight basal lamina structures around axons/Schwann cell units, and edema/swelling. Finally, we evaluate the ability to record single and multi-unit action potentials through microchannels permanently integrated with microwire electrodes in a terminal study after chronic implantation in the rat sciatic nerve. The chronic terminal electrophysiology experiment allows the testing of interfacing capabilities without needing to invest in the development of advanced wiring and packaging technologies for chronic continuous behavioral studies.

2. Materials and methods

2.1. Regenerative microchannel scaffold fabrication

To fabricate the regenerative microchannel scaffolds, a 40 μm PDMS (1:10 weight ratio Sylgard 184, Dow Corning) base layer was first spun on glass coated in titanium (10 Å) and gold (50 Å) for anti-adhesion. The PDMS base layer was then briefly treated with oxygen plasma to increase the adhesion between PDMS and SU-8. A 100 μm layer of SU-8 (SU-8 2100, MicroChem Corp) was then spun on top of the PDMS. The SU-8 was cured, exposed using an experimentally determined exposure dose of 520 mJ/cm^2, and developed forming the patterned microchannel walls on the PDMS base layer. The width and length of the microchannel walls were 20 μm and 10 mm, respectively. The width of the microchannels ranged from 50, 100, or 150 μm. The dimensions and spacing between the microchannel walls were controlled by the photolithography mask used for each microchannel type. The basic fabrication process of these steps is depicted in Fig. 2. Detailed methods for the fabrication of these steps can be found in literature [26].

Adding the top PDMS layer involved first spinning polyacrylic acid, a water resorbable layer, on another glass slide and drying it on a hotplate at 60 °C for 5 min. This was done twice. A 10 μm layer of PDMS was immediately spun on the polyacrylic acid (PAA) layers and partially cured on a hotplate at 65 °C for 4 min. During this time, the bottom PDMS layer with the SU-8 microchannel walls was treated with oxygen plasma to increase the adhesion between the two layers. The two glass slides were placed together with weight on top and baked on a hotplate at 60 °C for 30 min and then 90 °C for 1 h to ensure that the top PDMS layer was fully cured. Finally, the glass slide sandwich was soaked in water until the PAA dissolved and allowed for easy removal of the top glass slide. The basic process is depicted in Fig. 2. Once the layer of microchannels was removed from the glass slide, they were rolled perpendicularly to the direction of the microchannels and cut to 3 mm forming microchannel scaffolds with a cylindrical shape resembling that of the rat sciatic nerve. Each microchannel scaffold type was designed to contain a different number of microchannels based on the microchannel cross-sectional area. This was necessary in order to maintain a uniform rolled scaffold cross-section of approximately 1.5 mm across all three types of microchannel scaffolds. The 150 μm × 100 μm microchannel scaffolds contained 59 microchannels, the 100 μm × 100 μm microchannel scaffolds contained 84 microchannels, and the 50 μm × 100 μm microchannel scaffolds contained 143 microchannels.

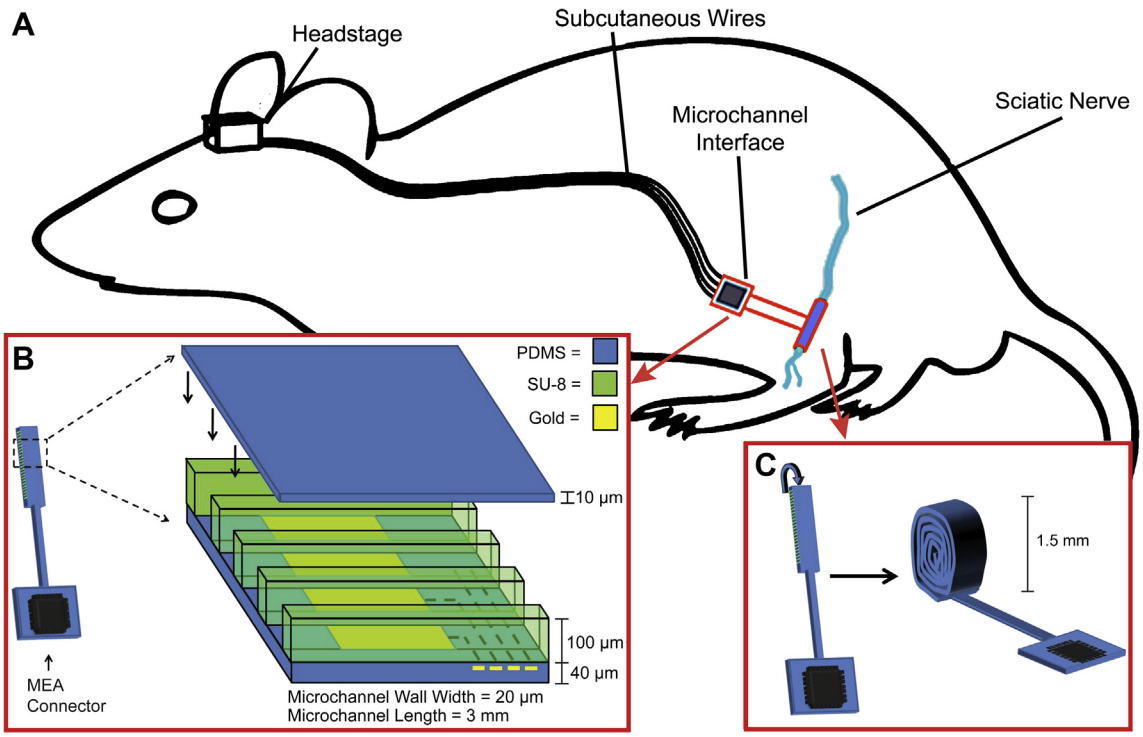

Fig. 1. (A) Overview of the rat amputee model depicting the site of implantation, tracing of subcutaneous wires, and percutaneous headstage for neural interfacing. (B) Schematic of microchannel architecture detailing materials, dimensions, and possible layout of incorporated gold electrodes. (C) Depiction of final microchannel scaffold after rolling for implantation. Adapted from Ref. [26].

2.2. Regenerative microchannel interface fabrication

The ends of eight insulated microwires (Stainless Steel 304, California Fine Wire Company) 60 μm in diameter and 10 cm in length were fed midway into eight random microchannels within the regenerative microchannel scaffold. 0.5 mm of each microwire end in the microchannel was de-insulated, forming the microchannel recording electrodes. The microchannel electrodes were inserted at the distal end of the regenerative microchannel scaffolds to minimally obstruct regeneration from the proximal side. Two coupled microwires were placed outside the scaffold running parallel to the microchannels with de-insulated electrodes at both ends of the 3 mm device forming a tripolar reference. This reference was held in place using standard silicone tubing placed around the reference and microchannel interface. This silicone tubing also served as a cuff to suture the proximal and distal transected nerves stumps into place during implantation. A second microwire reference was deinsulated by 0.5 mm and adhered to the outer wall of the silicone tubing using silicone adhesive (3140, Dow Corning®) forming a bipolar reference. This allowed the option of choosing either reference during electrophysiology experimentation.

2.3. In vitro cytocompatibility

Unrolled regenerative microchannel scaffolds lacking the PDMS cover layer were used for the *in vitro* experiments. Once fabricated, the 'open' regenerative microchannel scaffolds were placed at the bottom of tissue culture wells. Importantly, no protein coatings of any kind, such as laminin, were used. Lumbar dorsal root ganglia (DRGs) were explanted from P1 rat pups. The nerve roots were removed and the DRGs were placed on the open scaffolds at the entrance to the microchannels. For the first several hours, the DRGs were incubated with only a thin layer of DMEM/F12 media with 10% fetal bovine serum and 50 ng/mL nerve growth factor (NGF) (Roche). Subsequently, the wells were fully covered with the same media. The media, including NGF, were replaced every two days for a total of seven days. After seven days, the cultures of DRGs were fixed with 4% paraformaldehyde in PBS for 20 min and washed three times with 1X PBS. To visualize neurite outgrowth and non-neuronal cell migration, axons and Schwann cells of the DRGs were reacted overnight at 4 °C with antibodies to the 160 kDa neurofilament protein (1:500, mouse IgG1 NF160, Sigma) and S-100 (1:250, rabbit IgG S100, Dako), respectively, followed by secondary antibodies: goat anti-mouse IgG1 Alexa 594 (1:220, Invitrogen) and goat anti-rabbit IgG Alexa 488 (1:220, Invitrogen). Cell nuclei in the DRG cultures were marked by incubation in DAPI (Invitrogen) in PBS at a concentration of 10 μM for 15 min at room temperature. The fluorescently labeled cells and nuclei were visualized using a Zeiss upright microscope and the images were captured with an Olympus digital camera.

2.4. Microchannel scaffold implantation, explantation, and immunohistochemical preparation

A total of 18 regenerative microchannel scaffolds were implanted in the rat sciatic nerve amputee animal model, with an $n = 6$ for each of the three microchannel widths studied. In isoflurane anesthetized rats, the sciatic nerve was transected at the mid-thigh and the regenerative microchannel scaffold was sutured to the proximal and distal segments of the cut nerve. The nerve was then transected again, this time 2 mm distal to the distal end of the device and a large portion (approximately 1 cm) of the nerve distal to this second transection site was excised. The goal of this procedure is to leave a two mm 'distal nerve stump' attached to the distal end of the device so that regenerating axons may grow through the device in response to cues from the distal segment. By excising a segment of the nerve distal to this stump, we sought to prevent any regenerating axons from reinnervating their original targets. The net result is a sciatic nerve amputee model which forms a more stringent test for regenerative peripheral nerve interfaces than a conventional sciatic nerve transection and repair model.

After eight weeks, the regenerative microchannel scaffolds were explanted for histological analysis of axonal regeneration and nerve characterization. Explants were post fixed in 4% paraformaldehyde in PBS (Sigma–Aldrich) for 48 h at 4 °C and cryoprotected in 30% w/v sucrose in PBS for 72 h at 4 °C. Samples were then embedded in O.C.T compound (Tissue Tek) and stored at −80 °C. A 1.5 mm segment of nerve tissue distal to the microchannel scaffolds was sectioned in a transverse plane at 16 μm thickness with a cryostat (CM30505, Leica). Cross sections of the microchannel scaffolds with regenerated nervous tissue were made at 100 μm. These thicker sections were used to reduce mechanical stress and uncoiling which results from thinner sectioning. Sections mounted on slides were stored at −20 °C until staining.

2.5. Immunohistochemical analysis of microchannel scaffolds

Prior to staining, slides were brought to room temperature and excess O.C.T. surrounding the samples was removed with a razor blade. Next, an encompassing square section of precision mesh netting (McMaster-Carr) was applied over the whole cross section to prevent uncoiling of the microchannels during subsequent washes. The mesh netting was secured by applying a finite drop of cyanoacrylate glue at each corner onto the glass slide. Additional care was taken during subsequent reagent pipetting under a stereomicroscope to eliminate any air bubbles trapped in the mesh netting and to prevent uncoiling of the microchannels due to mechanical stress from excessive fluid flow. Microchannel slides were washed in PBS and then incubated in blocking solution for one and a half hours at room temperature. Blocking solution was prepared using a 1:25 dilution of goat serum (Gibco) with 0.5% Triton X-100 prepared in PBS. After incubation in blocking solution, the samples

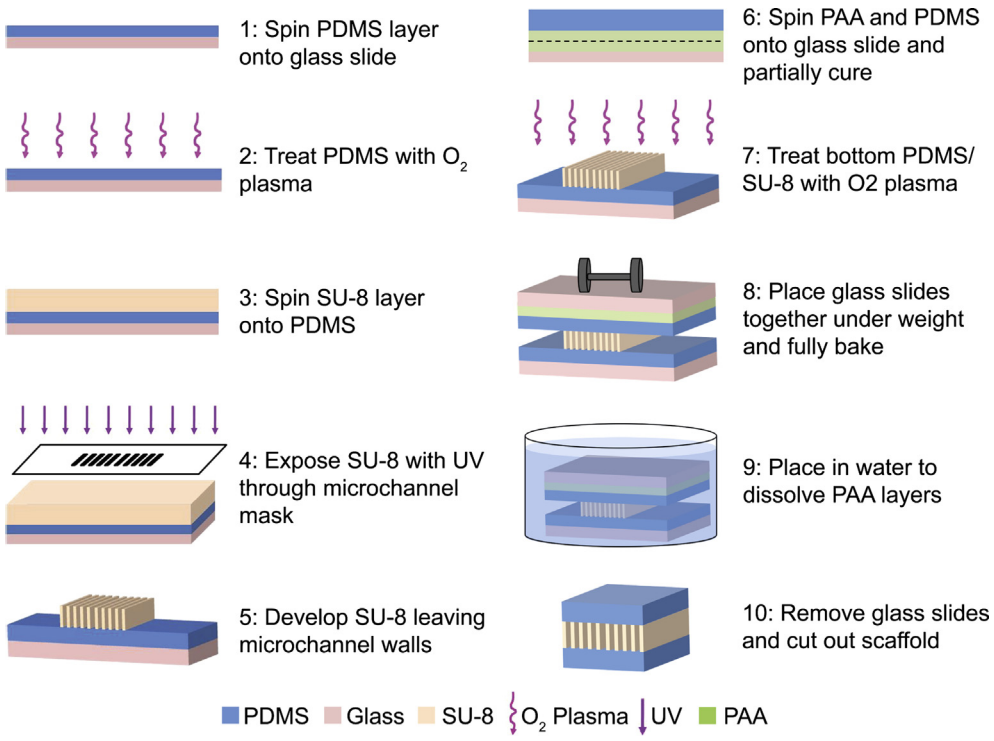

Fig. 2. Overview of all major fabrication processes for the regenerative microchannel scaffolds along with schematics depicting the device in each step. 'Open' microchannels from step 5 were used in *in vitro* studies. *In vivo* studies used microchannels from step 10. Drawings are not to scale.

were washed in a wash solution made of 0.5% Triton X-100 in PBS. The samples were incubated in primary antibody solutions (see above) for 24 h at 4 °C. Primary markers selected to stain for axons (NF160), Schwann cells (S100), and fibroblasts (1:500, mouse vimentin, Sigma–Aldrich) were prepared in blocking solution. The following day, the samples were again washed in wash solution and then incubated for 2 h in secondary antibodies at room temperature. Secondary antibodies used were goat anti-rabbit IgG Alexa 488 and goat anti-mouse IgG1 Alexa 594 and prepared in wash solution. Lastly, the samples were incubated with DAPI (see above), washed in PBS, and cover slipped using fluoromount-G (SouthernBiotech). It should be noted that the goal of the immunohistochemistry method used was to stain the superficial portion of the 100 μm thick tissue samples and not the entire tissue thickness as doing so was unnecessary for the analyses performed. Tile scan images of the samples were taken approximately 20 μm into the sample at 20×, 40×, and 100× magnification with a confocal microscope (LSM 510, Carl Zeiss) and stitched using Zen 2009 software (Carl Zeiss).

2.6. Immunohistochemical analysis of nerve tissue distal to the microchannel scaffolds

Glass slides with the 16 μm thick sections of nerve tissue distal to the microchannel scaffolds were brought to room temperature and rinsed three times in PBS to remove excess O.C.T. gel. Next, the samples were incubated in goat serum blocking solution for 1 h at room temperature, as described earlier. After blocking solution incubation, the samples were washed three times in wash solution and incubated overnight at 4 °C with primary antibodies. Primary markers were selected to stain for axons (NF160), Schwann cells (S100), fibroblasts (vimentin), and myelin (1:100, chicken IgY P0, Chemicon Intl.) each prepared in blocking solution. The following day, the samples were washed three times in wash solution and incubated for 1 h in secondary antibodies at room temperature. Secondary antibodies used were goat anti-rabbit IgG Alexa 488, goat anti-mouse IgG1 Alexa 594, and goat anti-chicken IgG1 Alexa 488 (1:220, Invitrogen); all were prepared in wash solution. After secondary antibody incubations, the samples were again rinsed in wash solution three times and then incubated with DAPI, washed, and cover slipped as described above. Samples were imaged at 20× and 40× magnification with an inverted microscope (Axiovert 200, Carl Zeiss). Tile scan images were taken at 20×, 40×, and 100× with a confocal microscope (LSM 510, Carl Zeiss).

2.7. Microchannel interface implantation and electrophysiology

A total of five regenerative microchannel interfaces were implanted in the rat sciatic nerve. In isoflurane anesthetized rats, the sciatic nerve was transected at the mid-thigh and the regenerative microchannel interface was sutured to the proximal and distal segments of the cut nerve. The microwire ends were led out through the musculature to lie subcutaneously in the local region. After 20 weeks (approximately five months) the rats were re-anesthetized lightly using isoflurane for induction followed by a ketamine/xylazine injection (i.p., 0.75 ml/kg). Booster shots of ketamine/xylazine (i.p., 0.25 ml/kg) were given as needed. The subcutaneous ends of the microwires were exposed and connected to a Cerebus Neural Signal Processing System (Blackrock Microsystems, USA) for signal acquisition. An 18 gauge needle was placed subcutaneously along the back of the rat serving as a distant low impedance reference.

Once the microwires were connected to the Cerebus System, spontaneous action potentials were recorded through the microchannel interface. Next, attempts were made to evoke sensory single unit action potentials using a variety of natural stimuli. These included brushing of the leg distal to the implant in the foot pad and toe region, pinching of the foot pad and toe region, ankle flexion/extension, and brushing of hair follicles distal to the implant. To control for movement related artifacts, identical sensory stimuli were delivered to the contra-lateral limb.

Lastly, the sciatic nerve was exposed near the sciatic notch using the same approach as the implantation surgery. A DS8000 stimulator (World Precision Instruments Inc, USA) was used to stimulate the sciatic nerve with 100 μsec, symmetric, charged balanced, bipolar, square wave voltage pulses at 0.33 Hz through a pair of stainless steel hook electrodes with 1.5 mm electrode spacing. A stimulus ramp of pulse amplitudes ranging from zero volts to 1 V at 0.01 V increments was used to evoke a range of neural responses, from a few action potentials to a general compound action potential. These were recorded through the microchannel interface.

All recorded signals were sampled at 30 KHz (33 μsec/sample) and first filtered in hardware using a 1st order high-pass Butterworth at 0.3 Hz and a 3rd order low-pass Butterworth at 7.5 KHz. Additional filtering was performed in software using a 4th order high-pass Butterworth at 250 Hz. Single unit action potentials were isolated online using conventional window discrimination spike sorting techniques based on spike amplitude and duration, and offline using an automated expectation-maximization algorithm though the Plexon Offline Sorter™ software package (Plexon, USA). Signal-to-noise ratios of isolated units were calculated by taking the average peak-to-peak amplitude of the unit and dividing it by 3 times the standard deviation of noise in that specific electrode.

2.8. Data analysis

Images from 100 μm thick histological sections through the scaffolding samples were used to analyze the number of microchannels containing axons, and number of axons and area of tissue occupied in each microchannel. The number of microchannels containing regenerated axons and the numbers of axons per microchannel across the three types of scaffolds were counted manually using ImageJ software. To evaluate the average amount of microchannels containing axons, for example in the

100 μm × 100 μm microchannel scaffolds, the percent of microchannels containing axons for each of the six 100 μm × 100 μm microchannel scaffolds were averaged together.

To evaluate the numbers of regenerating axons in each of the 100 μm × 100 μm microchannel scaffolds, up to 100 axon profiles per microchannel were counted. Using this data, the microchannels in each scaffold were categorized using arbitrary bins set at 0–10 axons, 11–100 axons, and 100+ axons. The percent of microchannels falling in these bins for the six 100 μm × 100 μm microchannel scaffolds are reported.

To evaluate the average free space in each microchannel within the 100 μm × 100 μm microchannel scaffolds, the tissue cross-sectional area in each microchannel was identified using the fibroblast stain as a proxy for the regenerated tissue cable. The area of positive staining for fibroblasts was measured and compared to the total microchannel cross-sectional area using ImageJ. These values were used to determine the percent area of a given microchannel filled with regenerated tissue. Similar to the axon counting analysis, data from the area analysis was used to categorize the microchannels of each scaffold into arbitrary bins of 0–25%, 25–50%, 50–75%, 75–100% microchannel area filled with tissue. The percent of microchannels falling in these bins for the six 100 μm × 100 μm microchannel scaffolds are reported.

Microchannels not structurally intact due to damage from sectioning and the associated tissue located within were not included in any analysis. Data from axon counts and tissue cross-sectional areas were analyzed using one-way ANOVA followed by a Tukey's least significant difference post-hoc test, where appropriate, to determine significant differences with at least 95% confidence.

3. Results

3.1. Regenerative microchannel scaffold

An image of the fabricated regenerative microchannel scaffold prior to the bonding of the PDMS cover layer (step 5 in Fig. 2) is shown in Fig. 3A. In this image a reflection of the SU-8 channel walls can be seen on the PDMS base layer. The SU-8 channel walls were successfully patterned using photolithography on the PDMS base layer and the SU-8 was capable of forming 20 μm by 100 μm channel walls. These 'open' microchannel scaffolds lacking the PDMS cover layer were used for all *in vitro* studies.

Application of the PDMS cover layer resulted in adherence to the top of the SU-8 microchannel walls forming arrays of closed microchannels (Fig. 3B). The PDMS cover layer is the thin line at the top of the microchannel walls. The arrays of microchannels were rolled perpendicular to the SU-8 walls forming the final regenerative microchannel scaffold for *in vivo* studies (Fig. 3C and D). The overall diameter of the scaffold was slightly larger than 1.5 mm. In these images, the SU-8 appears slightly gold and the PDMS appears gray or light blue. The microchannels are clearly visible. The dotted red line in Fig. 3D shows the separation between two layers of microchannels where the PDMS cover layer of the inner microchannel roll is in contact with the PDMS base layer of the outer microchannel roll. As a consequence of the rolling procedure, an unavoidable small open core was present in the center of the scaffolds (Fig. 3C).

Overall, three distinct types of microchannel scaffolds were fabricated where each had microchannel widths of either 50 μm, 100 μm, or 150 μm for chronic *in-vivo* studies. All microchannels had heights of 100 μm and lengths of 3 mm. It was observed however, that rolling the microchannel arrays to form the scaffolds resulted in slight inconsistencies in microchannel dimensions within a scaffold. Microchannels near the interior of the scaffolds tended to be wider than the peripheral microchannels. So, while each microchannel scaffold started with microchannel widths of 50 μm, 100 μm, or 150 μm, the rolling process created a range of widths within any given scaffold. A cross-sectional area comparison of the inner two rings of microchannels to the outer most ring of microchannels showed that this range was most apparent in the 50 μm × 100 μm microchannel scaffolds which had approximately an average 25% increase in microchannel cross-sectional area due to rolling. In contrast the 100 μm × 100 μm microchannel scaffolds and 150 μm × 100 μm microchannel scaffolds had a small increase of approximately 2.5% and 7.5%, respectively. In the end, this diversity of width provides an ability to study the effect of microchannel size in greater detail.

3.2. In vitro cytocompatibility studies

The cultured DRGs adhered well to the 'open' microchannel scaffolds. A representative DRG cultured on a scaffold with 50 μm wide microchannels stained for axons (red) and Schwann cells (green) is shown in Fig. 4. The microchannels are visible as dark horizontal lines separated by the faintly auto-fluorescent SU-8 microchannel walls. Immunoreactivity to axons (NF-160, red) and

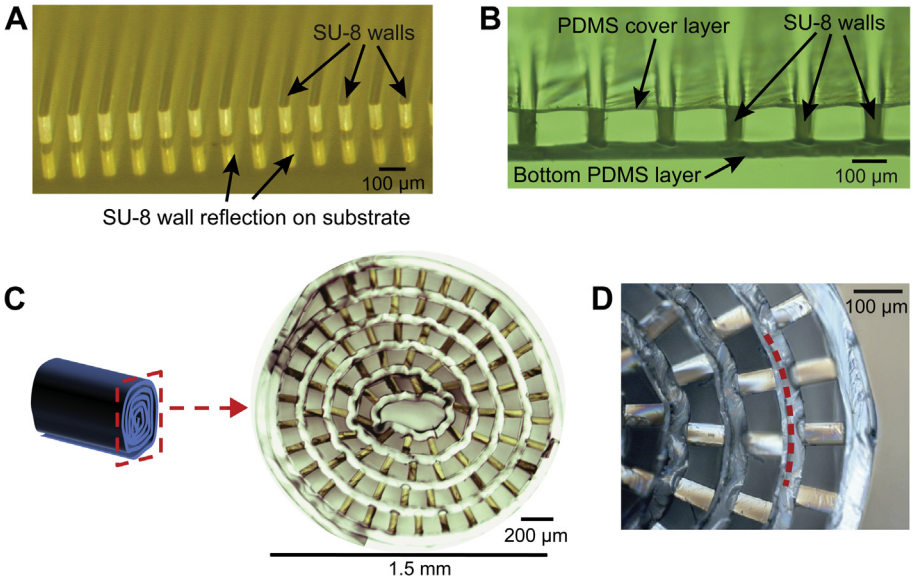

Fig. 3. (A) Image of 'open' microchannels corresponding to step 5 in Fig. 2. (B) Image of microchannels with the PDMS cover layer adhered to the SU-8 walls corresponding to step 10 in Fig. 2. (C) Cross-sectional view of 100 μm × 100 μm microchannel scaffold rolled for implantation. (D) Close up of rolled microchannel scaffold showing neighboring microchannel layers delineated by a red line. (For interpretation of the references to color in this figure legend, the reader is referred to the web version of this article.)

Schwann cells (S100, green) is shown in the main image of the figure, while the subset images show immunoreactivity to either axons (NF-160, red) or Schwann cells (S100, green). As seen from the main image, both axons and Schwann cells grew and proliferated in a robust manner out to 4 mm in length in some cases. Both axon extension and Schwann cell migration were aligned and oriented in the direction of the microchannels (Fig. 4 A, B). Neurite extension and Schwann cell migration from the explanted DRGs often appeared to be preferential towards the microchannels (Fig. 4C). While difficult to quantify, it was observed that more axon extension and Schwann cell growth occurred along the edges of the microchannels, on the SU-8 channel walls, as opposed to on the PDMS.

3.3. *In vivo* axon regeneration and dependence on channel cross-sectional area

Microchannel scaffolds with three different microchannel cross-sectional areas, 50 μm × 100 μm, 100 μm × 100 μm or 150 μm × 100 μm, were implanted for eight weeks to characterize the impact cross-sectional area has on nerve regeneration in a nerve amputee model. As mentioned previously, the 50 μm × 100 μm, 100 μm × 100 μm, and 150 μm × 100 μm microchannel scaffolds contained 143, 84, and 59 microchannels, respectively. Among the three channel dimensions, axon regeneration inside the 50 μm × 100 μm microchannels was significantly less than that through the 100 μm × 100 μm or 150 μm × 100 μm microchannels. Representative microchannel cross-sections of all three scaffold dimensions are shown in Fig. 5A. The microchannels in all three scaffold dimensions containing regenerated axons were analyzed. Fewer than half (50%) of the microchannels in the 50 μm × 100 μm microchannel scaffolds were populated with axons. On the other hand, a majority (greater than 95%) of the microchannels in both the 100 μm × 100 μm microchannel scaffolds and 150 μm × 100 μm microchannel scaffolds were populated with axons (Fig. 5B). In both the 100 μm × 100 μm and 150 μm × 100 μm microchannel scaffolds, axon regeneration within the open central core of the scaffolds was observed. These axon numbers were not quantified or included in the analysis.

Further analysis focused on the 100 μm × 100 μm microchannel scaffolds. A representative cross-section of a scaffold with discernible individual axon profiles is shown at higher magnification in Fig. 5C. Axon profiles per microchannel were counted up to 100 and the results are graphically depicted in Fig. 5D using arbitrary bins set at 100+ axons, 11–100 axons, and 0–10 axons. On average, approximately 30% of all analyzed microchannels contained more than 100 axons, 40% microchannels contained 11–100 axons, and 30% of the microchannels contained fewer than 10 axons. There was no observable dependence or variation of axon regeneration to the slight changes in microchannel cross-sectional

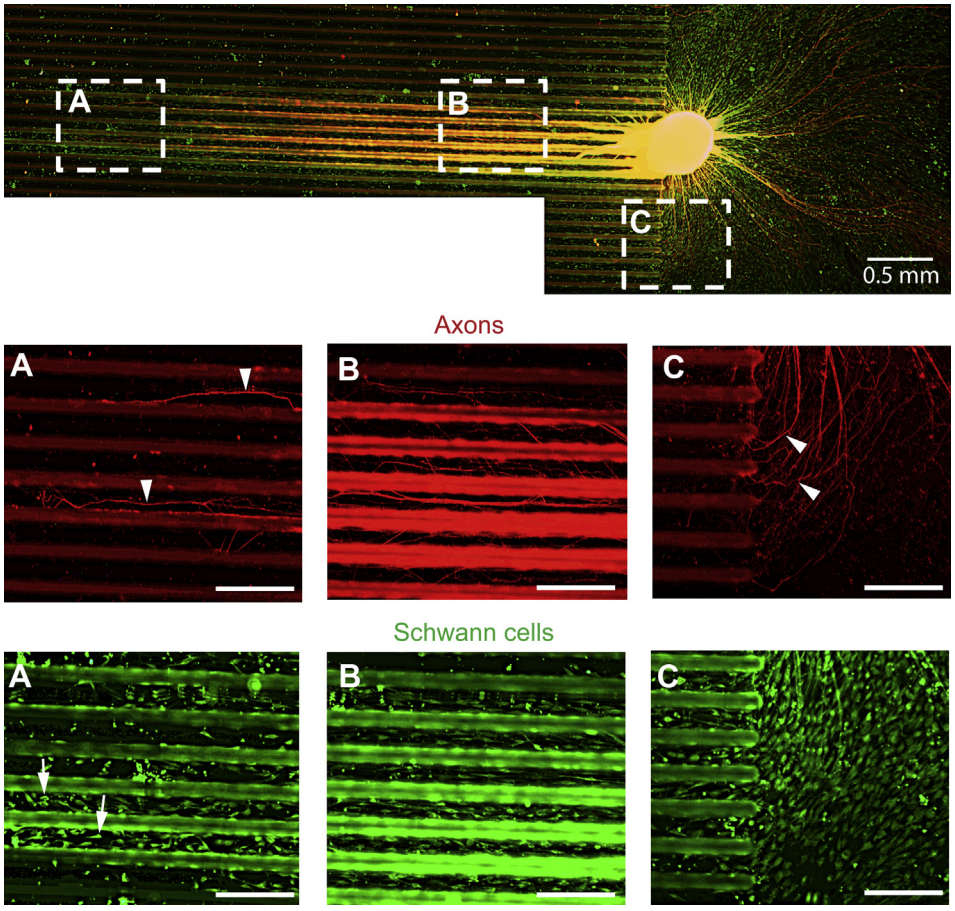

Fig. 4. (Main image) DRG *in vitro* culture with axon processes and migrating Schwann cells on 'open' 50 μm wide microchannels. (A) and (B) Axons and Schwann cells were aligned and oriented in the microchannels and grew/migrated out to 4 mm in some cases. (C) Growth and migration of axons and Schwann cells re-orienting towards the microchannels. Axons (red); Schwann cells (green); DRG and regions of axon/Schwann cell co-localization appear orange/yellow; Microchannels are visible as dark horizontal regions separated by auto-fluorescent SU-8 microchannel walls; Arrowheads indicate axons; Arrows indicate Schwann cells; Scale bar = 200 μm unless otherwise noted. (For interpretation of the references to color in this figure legend, the reader is referred to the web version of this article.)

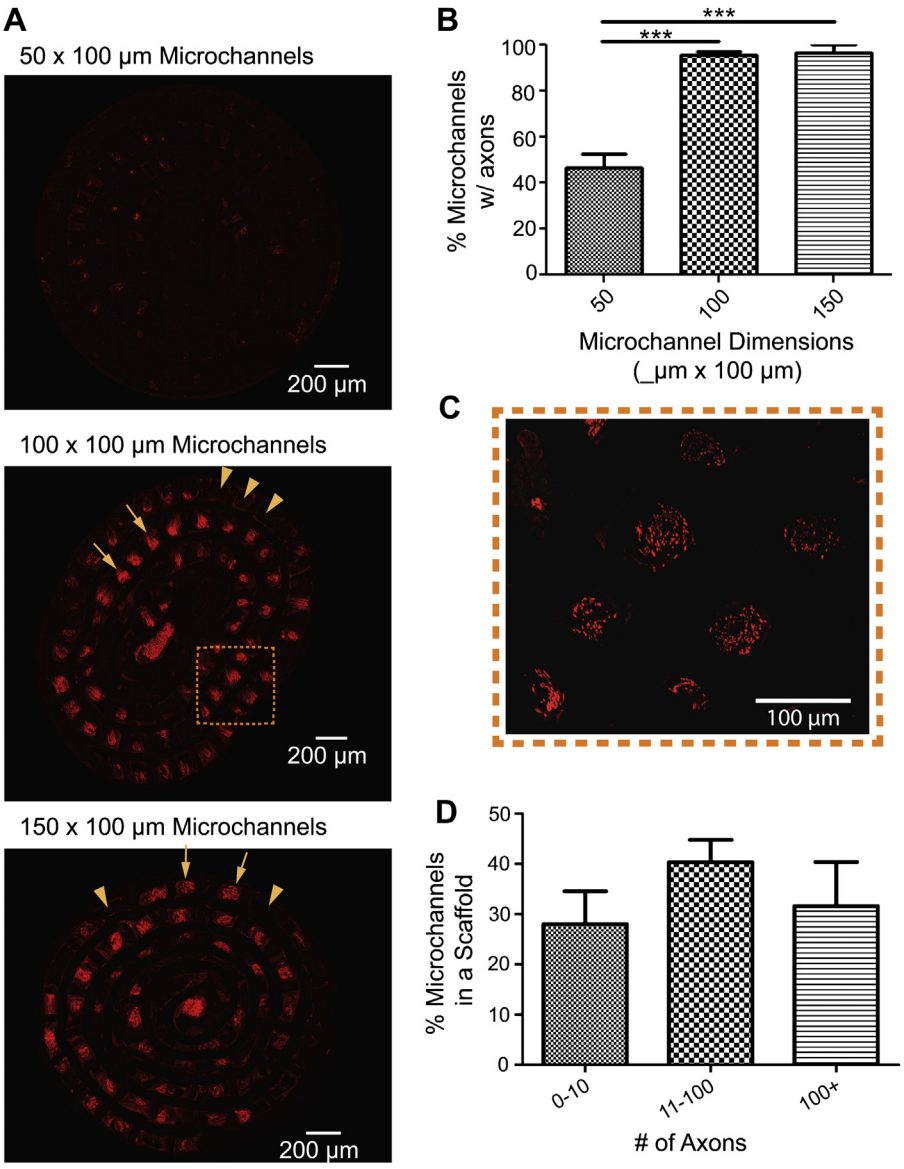

Fig. 5. (A) Representative cross-sectional comparison of axon (red) profiles through the scaffolding among the three different microchannel dimensions: 50 µm × 100 µm; 100 µm × 100 µm; 150 µm × 100 µm, respectively. Cross-sections were taken at the midpoint of each scaffold. Arrows indicate microchannels containing axons. Arrowheads indicate microchannels lacking axons. (B) Quantitative analysis on the percent of microchannels in a scaffold containing regenerated axons for each microchannel dimension. (C) Close up of 100 µm × 100 µm scaffold cross-section depicting single axons profiles within microchannels. (D) Quantitative analysis on the percent of microchannels within the 100 µm × 100 µm microchannel scaffolds containing axon populations of 0–10, 11–100, or 100+ axons. (Mean ± S.E.M., ***$p < 0.001$). (For interpretation of the references to color in this figure legend, the reader is referred to the web version of this article.)

area due to rolling or on spatial location of the microchannel within the scaffold.

3.4. Space for future axon maturation

Analyses were performed to evaluate free space in the microchannels available for axon maturation over time. Accordingly, the area occupied by the regenerated tissue cable was compared to the area of the microchannels in the 100 µm × 100 µm microchannel scaffolding samples. Staining for fibroblasts was used to calculate the area of the regenerated cable (Fig. 6A). A close-up of the cross-section along with delineations of the tissue and microchannel area are shown in Fig. 6B. Approximately 95% of all microchannels containing tissue in the 100 × 100 µm^2 microchannel scaffolds were observed to have at least 25% free cross-sectional area remaining (Fig. 6C).

3.5. Distal nerve morphological analysis

The response of the nerve to induced guidance from the microchannel architecture was characterized using immunofluorescence for fibroblasts and basal lamina. In cross sections of the nerve tissue distal to the microchannel scaffold there was evidence of reorganization into 'microchannel fascicles', similar to typical nerve fascicles. These microchannel fascicles were characterized by defined perineurial-like sheaths of fibroblasts hosting aggregates of regenerating axons and Schwann cells (Fig. 7C) and supportive extracellular matrix (Fig. 7D). Additionally, an epineurial-like layer successfully reformed around the whole regenerating nerve

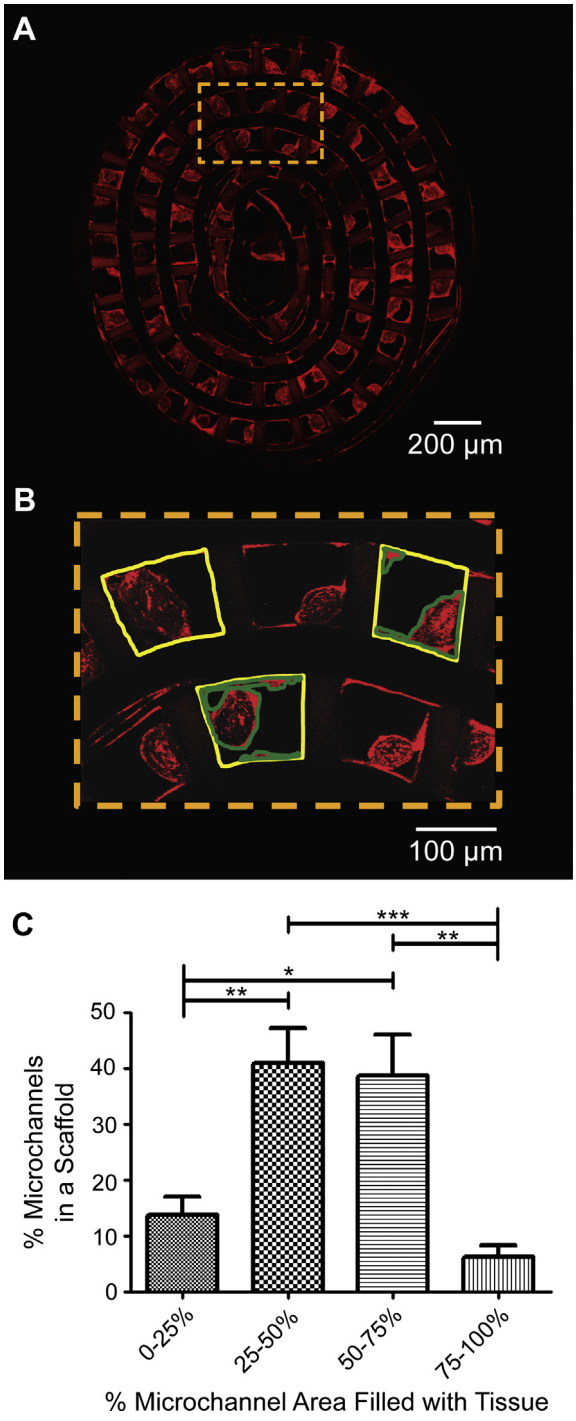

Fig. 6. (A) Representative cross section of 100 μm × 100 μm microchannel scaffold stained for fibroblasts (red). Cross-sections were taken near the midpoint of the scaffold. (B) Close-up of microchannels with delineations of microchannel area (yellow) and positive fibroblast staining used as a proxy for tissue cross-sectional area (green). (C) Quantitative analysis on the percent of microchannels within the 100 μm × 100 μm microchannel scaffolds with 0–25%, 25–50%, 50–75%, and 75–100% area filled with tissue. (Mean ± S.E.M.,$^{*}p < 0.05$, $^{**}p < 0.01$, $^{***}p < 0.001$). (For interpretation of the references to color in this figure legend, the reader is referred to the web version of this article.)

characterized by concentric fibroblast organization (Fig. 7C). The aggregates of axons and Schwann cells corresponding to the microchannel architecture were observed up to ~1 mm distal to the implant (Fig. 7A). This distance coincided approximately with the end of the distal attached nerve segment. As expected, during nerve regeneration, sprouting of axons was visually observed as indicated by the evident increase of axon profiles progressively distal to the scaffolding (Fig. 7A). Additionally, overall nerve regeneration was observed to be unidirectional and organized (Fig. 7A). There were no signs of aberrant, unorganized axon regeneration and/or bulbous nerve swelling distal to the microchannel scaffold.

3.6. Distal axon regeneration analysis

At a closer inspection of the extracellular matrix, evident reformation of the basal lamina and endoneurial tubes was observed tightly surrounding all the axons and accompanying Schwann cells within the distal segments of the nerve (Fig. 8A). Immunofluorescence for Schwann cells identified the abundant presence of Schwann cells within the microchannel fascicles (Fig. 8B) accompanying the regenerated axons. Further immunofluorescence showed at least a portion of the Schwann cells were of the myelinating phenotype and had re-deposited myelin on axons providing insulation for normal nerve conduction (Fig. 8C). In general, the nerve cross-section contained a uniform distribution of tissue without large edema like voids that lack both cells and extracellular matrix within the nerve.

3.7. Regenerative microchannel interface

The microchannel interfaces utilized 60 μm diameter microwires as the recording electrodes. Due to the size of the microwires and based on the results from axon regeneration into the 100 μm X 100 μm microchannel scaffolds, the 150 μm X 100 μm microchannel scaffolds were chosen for interfacing. This ensured the space within the microchannels containing a microwire was close to, but not less than 100 μm X 100 μm. The recording electrodes were positioned in the middle of the microchannels and were 0.5 mm long. A proximal, distal, and side view of a representative microchannel interface is shown in Fig. 9A–C, respectively.

3.8. Spontaneous and sensory evoked single unit action potential recordings

Spontaneous and/or sensory evoked single unit action potentials could be recorded from all microchannel interfaces after five months of implantation. Out of the 40 electrodes from the 5 devices, 9 were non-functional due to broken microwire leads leaving 31 electrodes that could be used for recording activity. Recordings from 8 of the 31 functioning electrodes were found to contain single unit action potentials. Peak to peak amplitudes of the action potentials ranged from approximately 30–80 μV. Thus regenerated axons in the microchannel interfaces were functional and had successfully innervated the most distal regions of the leg and foot. A variety of sensory stimuli were capable of producing single unit action potential activity across all animals including ankle flexion/extension, pinching and rubbing of the foot pad and toe region, and hair follicle brushing. In general, ankle flexion/extension produced the largest and most reliable action potentials across all animals.

A representative sensory evoked action potential recording from a single microchannel is shown in Fig. 10. This action potential is believed to be from an afferent sensory fiber, likely a proprioceptive axon reinnervating a muscle spindle or golgi tendon organ based on responsiveness to plantar flexion. The action potential wave form, isolated using window discrimination and an automated expectation-maximization algorithm through the Plexon Offline Sorter™, is shown in Fig. 10A. A typical tri-phasic appearance reported elsewhere for recordings taken within microchannels is

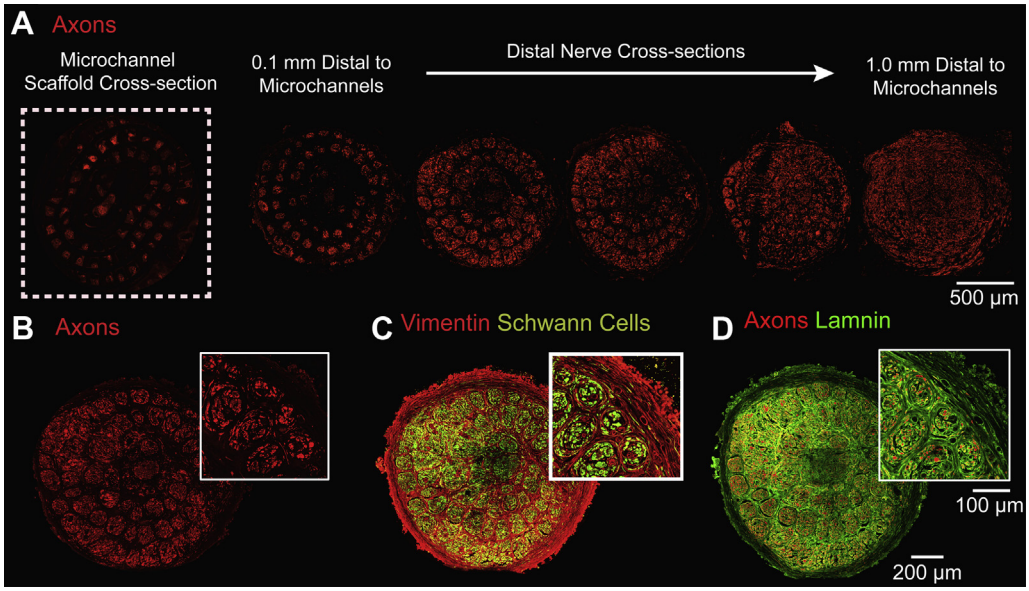

Fig. 7. (A) Distal nerve cross-sections stained for axons (red) at increasing distances away from the scaffold (left image is the scaffold mid-section for reference). (B–D) Nerve cross-sections distal to the scaffolding. (B) Close-up of distal nerve cross-section stained for axons (red) showing aggregates of axons. (C) Distal nerve cross-section stained for fibroblasts (red) and Schwann cells (green/yellow) showing perineurial-like structures. (D) Distal nerve cross-section stained for laminin (green) and axons (red) showing basal lamina and connective tissue. (For interpretation of the references to color in this figure legend, the reader is referred to the web version of this article.)

noted in the waveform [11,13]. Fig. 10B shows the raw recorded signal during plantar flexion held over 4 s in an 8 s time window where the flexion was released at time = 61 s and is denoted by a motion artifact. Fig. 10C shows a plot of firing rate over a longer duration where the plantar flexion was held for 60 s, released for 30 s, held for 60 s, and again released for 30 s. Robust and steady firing of action potentials was observed during the flexion periods in contrast to the lack of firing during the release periods. The average peak to peak amplitude of this unit was measured to be 54 μV with an average SNR calculated to be 2. There was no activity in response to control sensory stimulation of the contralateral leg for this unit or any other sensory evoked unit across all animals.

3.9. *Electrically evoked multi unit action potential recordings*

The presence of evoked multi-unit activity recorded from the microchannel electrodes at five months was used to calculate the number of electrodes per device that could be used for successful recordings, which we have termed 'device viability'. Evoked multi-unit activity was observed on an average from 4.5/8 electrodes per device, which corresponds to a mean device viability of 56.25% (SD 12.5%) after the five months of implantation. It should be noted that this mean viability *includes* nine electrodes with broken microwire leads. These nine electrodes were deemed non-functional after the broken microwire leads were visually verified and by a lack of an electrical stimulation artifact present on all functional electrodes. In one device all of the electrodes contained evoked multi-unit activity except those which were deemed non-functional.

The ramped voltage stimulation evoked increasing levels of multi-unit activity with increasing recruitment of axons within the microchannels. The peak to peak amplitudes ranged from approximately 260–520 μV near the upper threshold of stimulation. The amplitudes and waveforms of the multi-unit microchannel action potentials varied between animals and microchannel interface electrodes; however, in all cases signals were clearly distinguishable and did not require averaging to detect. Furthermore, the differences in multi-unit microchannel action potential amplitudes, latencies, and waveforms across electrodes and animals indicated there were different axon populations that regenerated into each of the respective microchannels, which was expected. In all animals, electrical stimulation via hook electrodes produced visible contractions of the gastrocnemius muscles and ankle extension, indicating successful nerve regeneration and functional reinnervation of distal targets.

Representative electrically evoked multi-unit activity from three electrodes of a single microchannel interface using the 0–1 V stimulus ramp is shown in Fig. 11. As just noted, different multi-unit microchannel action potentials were found in all three channels (and others not shown). Additionally, the recruitment of different units adding to the multi-unit microchannel action potentials can be seen in all three electrode recordings as the voltage stimulus was increased.

4. Discussion

One of the major challenges in the area of neural interfacing is to develop reliable devices that establish neuronal communication for prosthetic control. There have been many efforts towards this endeavor that can be broadly categorized into central neural interfacing or peripheral nerve interfacing. The efforts in these areas to restore, at least partially, sensorimotor function predominantly hinges on developing interfaces that can restore communication through neuronal recording and stimulation. While cortical neural interfacing is plagued by challenges of interfacing with the brain and decoding abstract signals intended for functional restoration, peripheral nerve interfacing has the potential to obtain signals that are more closely related to the intended muscle activation and are significantly less invasive. The culmination of a number of peripheral nerve interfacing studies has resulted in the development of interfaces such as cuff, penetrating and regenerative sieve electrodes [1–7]. While being helpful to some extent, these interfaces have drawbacks ranging from lack of selectivity in the case of the cuff electrode to more severe consequences in the case of the penetrating USEA where the interface implantation leads to inflammation and generation of scar tissue [1–5]. The present study was focused on development of a device that would

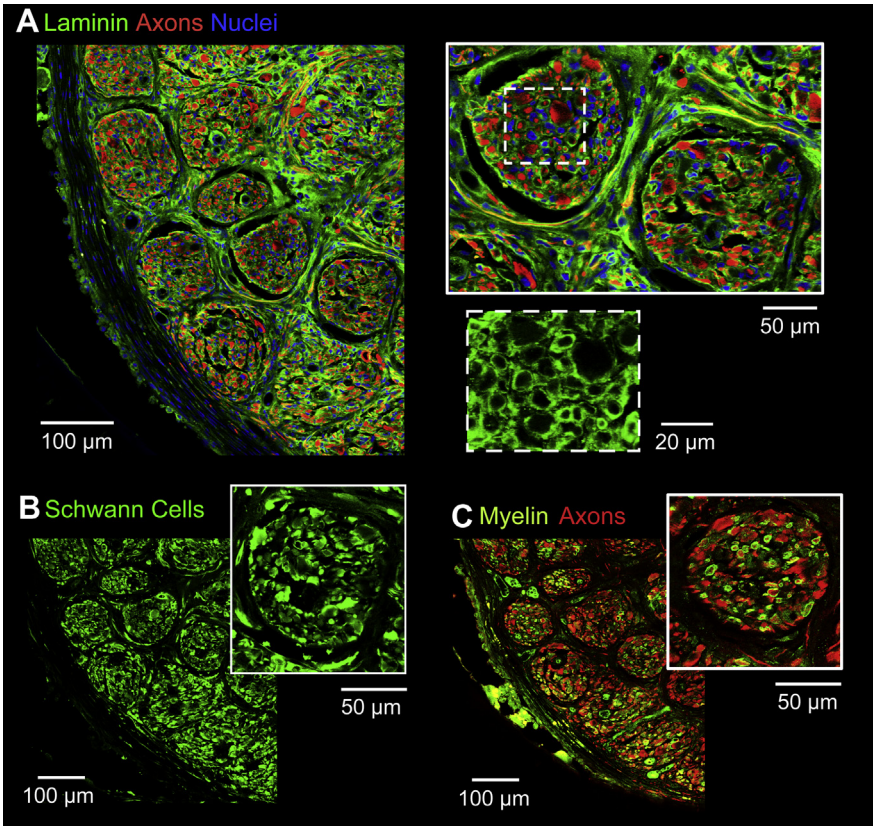

Fig. 8. (A) Close up of distal nerve cross section stained for laminin (green), axons (red), and cell nuclei (blue). Microchannel fascicles shown in the top right insert. Bottom right insert depicts a close up of the basal laminae structure. (B) Aggregates of Schwann cells (green) and (C) re-myelinated axons, shown by co-localization of myelin (green) and axons (red), were spatially correlated within microchannel fascicles. (For interpretation of the references to color in this figure legend, the reader is referred to the web version of this article.)

be effective as an interface for amputees with the potential for long term utility and minimal adverse effects.

One of the key features of the design strategy was to take advantage of the regenerative approach using microchannels and materials non-toxic to the peripheral nervous system including PDMS and SU-8. A simple and common fabrication technique was developed for scaffold production and involved initially generating flat sheets of microchannels which were subsequently rolled into conduits mimicking the size and fascicular organization of the rat sciatic nerve (Fig. 3). This simple fabrication methodology should tremendously help in the large scale production of these devices.

However, one of the limitations of this approach is that the procedure creates a small open core in the center of the rolled microchannel scaffold. Even though one could pursue ways to occlude this space [13], this was not initially considered because it would hinder overall regeneration. If it was found that a disproportionate number of axons regenerated through the central core instead of the microchannels, occluding the hole would have been critical. As this scenario did not occur, occluding the central core was not pursued. Another issue with the rolled approach was the inconsistency in the cross-sectional area of each microchannel from the center of the scaffold moving outwards radially. The cross-sectional area tended to increase slightly towards the center of the scaffold. However, this change in microchannel cross-sectional area within the scaffolds (2.5% in the 100 μm × 100 μm microchannel scaffolds) did not significantly impact the performance of the device, unlike the three distinct microchannel widths evaluated, and hence was not rectified in the current study. In future

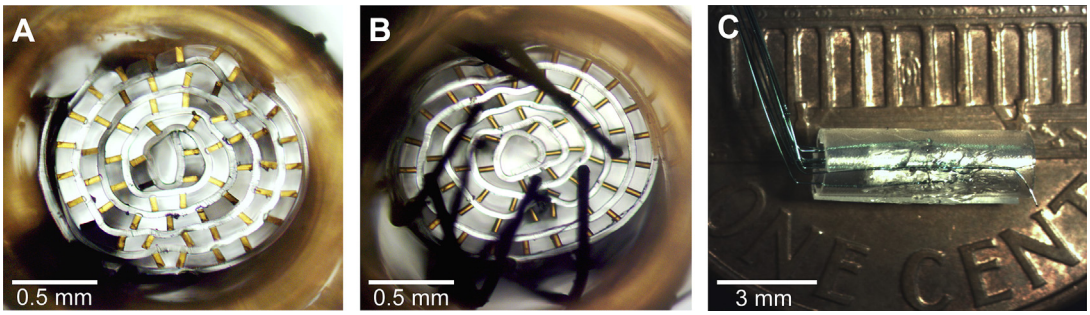

Fig. 9. Images of a representative microchannel interface with microwire electrodes. (A) Proximal view. (B) Distal view with microwire electrodes entering the microchannels. (C) Side view.

modifications of the device, this issue can be resolved by decreasing the spacing of the SU-8 walls in the inner region of the device.

There are additional advantages of using the rolling approach to generate the microchannels. First, the size of the scaffold is easily scalable to nerves of different diameters. If the nerve is larger, the sheet simply needs to be longer (more microchannels) in order for the rolled scaffold to have an increased diameter. Another benefit is that the number of microchannels available for interfacing scales accordingly for larger nerves. This is especially important when dealing with upper arm or upper leg amputees where the larger amputated nerves contain significantly more relevant information needed to control a neural prosthetic.

Additionally, an important finding of this study is that the components of the microchannel device were non-toxic to both DRG neurites and Schwann cells without needing any extracellular protein coating, such as laminin. The *in vitro* experimentation also showed the microchannel design was capable of guiding and directing neurites and Schwann cells as judged by the unidirectional neurite outgrowth and Schwann cell migration along and through the microchannels (Fig. 4A, B). Further, it was interesting to note that neurites and Schwann cells initially growing and migrating perpendicular to the microchannels changed their initial direction and re-oriented towards the microchannels (Fig. 4C). This suggests the presence of an, at this time, unknown mechanism for preferential growth/migration towards the microchannels. However, this was not the case with neurites and Schwann cells farther away from the microchannels, suggesting a spatial dependence. There was also preferential growth on the SU-8 microchannel walls. However, this was fairly inconsequential *in vivo* because the microchannels were covered with the top PDMS layer thereby containing the axons within the microchannels regardless of which surface they preferred.

In vivo experimentation with the microchannel scaffold to assess potential for chronic interfacing in amputees brought to light a number of additional significant observations. First, the implants were well tolerated in all cases with little to no scar tissue, in general. Second, robust numbers of axons were observed in the 100 μm × 100 μm and 150 μm × 100 μm microchannels showing that these microchannel scaffolds readily support nerve regeneration despite lacking distal reinnervation targets. The microchannels in the 100 μm × 100 μm microchannel scaffolds did have varying numbers of axons ranging from a handful in some cases to many hundreds in others (Fig. 5D), but seldom were completely lacking axons altogether (Fig. 5B). Furthermore, the 100 μm × 100 μm microchannels were at or near the lower boundary for microchannel sizes capable of supporting axon regeneration as judged by the poor regeneration in the 50 μm × 100 μm microchannels (Fig. 5A, B). With regards to both the 100 μm × 100 μm and 150 μm × 100 μm microchannels, it was observed anecdotally that microchannels completely lacking axon growth tended to occur near the periphery or in the outer rings of the scaffold. This was expected based on the typical nerve regeneration pattern where preferential regeneration occurs along the Bands of Büngner which form a central cord occurring roughly near the center of scaffolds [27–29]. Given the robust regeneration across these scaffolds though, microchannels lacking axons were very infrequent and

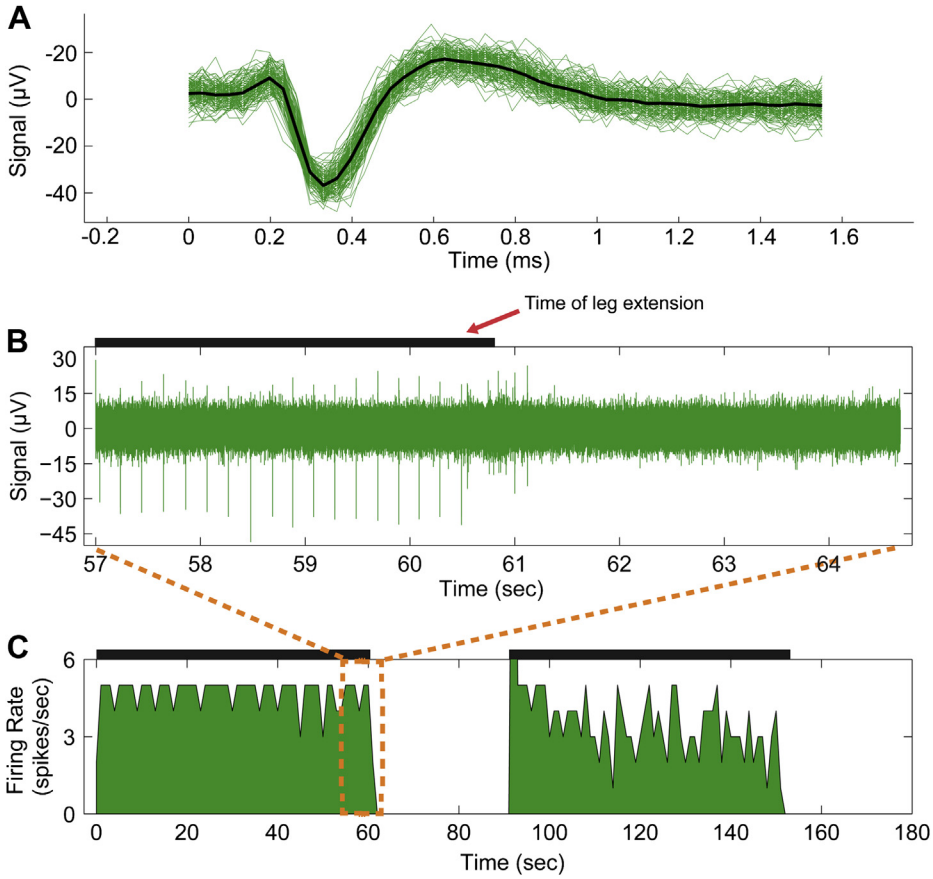

Fig. 10. Representative sensory evoked single unit action potential recording through an electrode in a microchannel interface. (A) Action potential waveform. (B) Raw recording signal over 4 s of plantar flexion followed by 4 s lacking plantar flexion. Plantar flexion was released at time = 61 s and is denoted by a motion artifact during release of the ankle. (C) Spike rate of the action potential where plantar flexion was held for 60 s, released for 30 s, and repeated. A 1 s bin size was used to generate the plot.

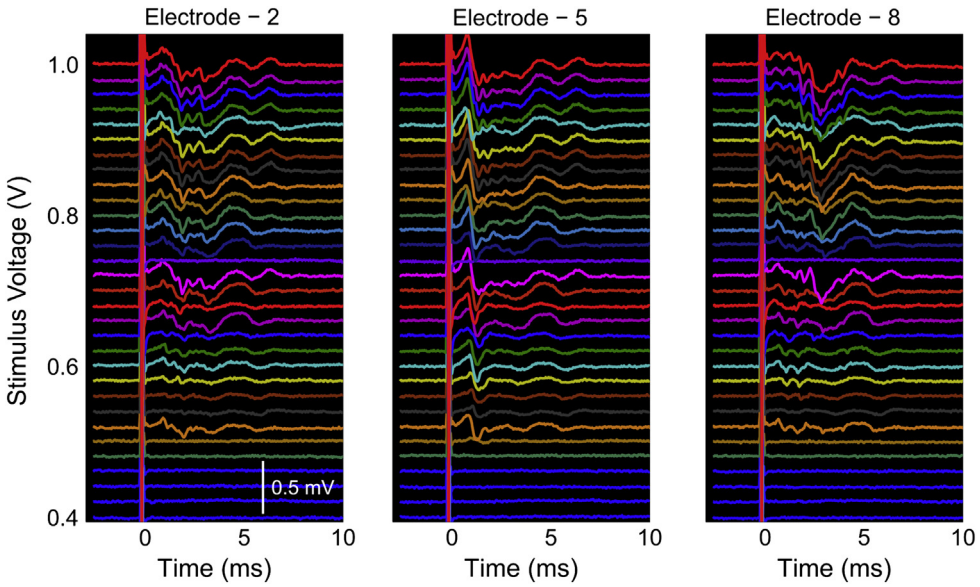

Fig. 11. Representative electrically evoked multi-unit activity with different amplitudes, latencies, and waveforms from 3 representative electrodes in a microchannel interface.

would be difficult to predict prior to implantation. Besides the few microchannels lacking axon regeneration, no trends of greater or lesser axon regeneration dependent on microchannel location (center vs. periphery of the scaffold) or any other discernible topographical pattern were observed. It is also important to note that these trends of regeneration and dependence on microchannel size agree well with other studies looking at non-amputee scenarios [13,30].

For the *in vivo* studies, the rationale for choosing 100 μm × 100 μm microchannels for detailed analysis was based on the need to use the smallest possible microchannel cross-section to increase the amplitude of an axon's AP while still maintaining reliable regeneration in a majority of the microchannels. In the implantations with this device, a vast majority of the microchannels had at least 25% of the original cross-sectional area remaining for future maturation of axons, Schwann cells, and the supporting tissue in general (Fig. 6). A significant increase in regenerating axon numbers is not expected to occur within the microchannels given that an eight week time point was chosen for analysis. Another important point is that this analysis does not take into account the axon pruning that will occur at later time points resulting in fewer axons in the microchannels. This validated that axon constriction, as observed in the Sieve electrode [7,31], should not be a major concern when microchannel sizes similar to those in this study or larger are used in peripheral nerve interfacing applications. There was a small subset of microchannels, 5%, in which greater potential for future axon constriction might be expected, due to their being filled more than 75% with tissue when these scaffolds were explanted. However, the actual occurrence of axon constriction in this small subset would have to be assessed at significantly later time points to account for axon pruning, as previously mentioned. It is also important to note that even if axon constriction occurred in these few microchannels, it would not drastically affect the interfacing capabilities of the scaffold due to the overall number of microchannels presenting numerous opportunities to record from other axons.

Analysis of the nerve and axons distally as they regenerated out of the implanted microchannel scaffold also revealed a number of interesting details. The basic structure of the nerve stump distal to the scaffold had been reorganized in response to and matching the architecture of the proximal microchannels (Fig. 7). This was first observed with the axons and Schwann cells that were grouped and organized according to the proximal microchannels (Fig. 7B, C). In addition to the axon and Schwann cell organization, connective tissue layers similar to those observed in a normal nerve had reformed. A stereotypical uninjured nerve is morphologically compartmentalized by epineurial, perineurial, and endoneurial connective tissues [15,32,33]. What was observed in this study was the reformation of all three types of connective tissue in the regenerated nerve distal to the implant. An epineurial like sheath surrounding the whole nerve cross section could be identified by concentric fibroblast arrangements. Furthermore, as a result of the re-organization within the distal nerve, multiple perineurial like sheaths forming 'microchannel fascicles' marked by concentric fibroblast arrangements around the aggregates of axons and Schwann cells was observed (Fig. 7C). These ring like sheaths of fibroblasts correlated with the presence of extracellular matrix shown by the lamellae support structure (Fig. 7D). This is similar in nature to the perineurium of a stereotypical nerve which has been noted for its concentric layers of flattened cells with prominent basement membranes [15,33]. In general, the microchannel architecture facilitated and encouraged parallel nerve fiber growth by directing axon regeneration through the microchannels and producing an organized microchannel fascicle morphology. The reformation of endoneurial connective tissue is discussed in a later paragraph.

It was also evident that the 'microchannel fascicles' maintained their morphology as much as 1 mm distal to the scaffolding. With distance, the fascicles gradually lost their perineurial structure and the axons gradually disassociated from the microchannel morphology to a homogeneous morphology. However, the axons still maintained a general, unidirectional growth (Fig. 7A) and eventually branched out into the local muscle bed (data not shown). It is also important to consider previous work which has shown that muscle reinnervation, while a key component for functional nerve regeneration across critical gaps, is not necessary for nerve stability. In fact there has been no evidence of motoneuron death after chronic axotomy in nerves and axons lacking their reinnervation targets out to 14 weeks [34]. Furthermore, nerves and axons retain a regenerative capability and can

functionally reinnervate muscles after long periods such as 12 months of chronic axotomy, albeit a reduced number of regenerating axons over long distances, but with similar functional outcomes compared to controls [35–37].

While the macroscopic structure of the distal nerve changed significantly, the axons, Schwann cells, and associated connective tissue were undergoing the normal regenerative processes. Similar to the perineurium in a normal nerve, endoneurial connective tissue is heavily associated with basal lamina for structural support and cell adhesion between axons and proliferating Schwann cells. Proliferating Schwann cells are crucial for nerve regeneration by forming conduits and providing a favorable environment for subsequent axon elongation, maturation, and long term Schwann cell-axon pairing [15,25,29,32,33,38]. Such conduit like structures of connective tissue were visualized in each individual microchannel fascicle by laminin staining, as indicated by the porous texture. Accordingly, each mature Schwann cell and axon pair was invested with a tight basal lamina structure and encompassed by extracellular matrix (ECM), forming endoneurial tubes (Fig. 8A). In a regenerated nerve, mature Schwann cells play a crucial role by providing aid in the conduction of nerve impulses and providing trophic support for neurons [15,29,32,38]. Further, it was revealed in the analysis of myelin and Schwann cell staining that many axons were re-myelinated and a majority were closely associated with Schwann cells, thus suggesting the presence of both myelinating and non-myelinating Schwann cell phenotypes (Fig. 8B, C). With regard to the general tissue distribution, immunohistochemistry indicated that large edema filled voids lacking cell populations and extracellular matrix within regions of the nerve were absent (Fig. 8A). Together these observations support the finding that microchannels are supportive of the proper initial microenvironment for basal lamina/connective tissue deposition by proliferating Schwann cells and for chronic stability of the regenerated healthy nerve.

Not only do these observations support chronic stability of the regenerated nerve with the device, but they also suggest that neuroma formation may not be a concern for use of this device in the amputee population. The regenerating nerve and axons, lacking distal reinnervation targets, displayed opposite characteristics to those most commonly associated with neuromas after being constrained to regenerate through the device. Neuromas are characterized by aberrant, random regeneration and highly disorganized axon distribution resulting in the commonly observed bulbous nerve swelling [17,18,22,25] which occurs as early as 1 week post nerve transection leading to chronic complications [18,22,25]. However, quite the opposite was observed in this study as shown by the microchannel fascicle morphology, general unidirectional growth of regenerating axons distal to the device, and lack of bulbous nerve swelling (Fig. 7). Additional axonal characteristics within neuromas include a lacking Schwann cell population and myelination of axons [17,18,22], loose basal lamina structure surrounding axon/Schwann cell units [22,23], and endoneurial edema within the nerve structure [17,19]. Again, quite the opposite was observed in this study. An abundant population of Schwann cells closely associated with myelinated axons was observed. Furthermore, a tight, supportive basal lamina structure surrounded the axon/Schwann cell units and there was no presence of large voids within the nerve structure indicating an absence of edema or swelling (Fig. 8).

In addition to the chronic stability of the microchannel scaffolds observed in an amputated nerve, both spontaneous and sensory evoked single unit activity were successfully recorded *in vivo* using the permanently integrated electrodes at the chronic time point a full five months after implantation. Thus indicating that the devices are both durable and that regenerating axons in them are viable over prolonged periods. The sensory evoked single unit action potentials included a multitude of activity originating from the distal foot pad region suggesting at least partial reinnervation of distal targets and potentially the recovery of proprioceptive, nociceptive, and other sensory perception. Additionally, multi-unit action potentials were recorded through all microchannel interfaces in response to proximal electrical stimulation (Fig. 11). Observed contractions of the gastrocnemius muscles and plantar flexion in response to the electrical stimulation further suggest reinnervation of distal targets and potentially some recovery of motor function.

While it is challenging to record single unit action potentials from regenerated axons in anesthetized rats, eight of 31 functioning electrodes were successfully used towards this end. Furthermore, it is highly unlikely that all sensory afferents were stimulated even though a variety of sensory stimuli were used. So it is possible single unit action potentials could have been recorded through additional electrodes. Additional attempts were made using electrical stimuli to evoke single unit action potentials, but small levels of multi-unit activity were consistently observed even at low stimulation levels. The inability to evoke single unit action potentials is attributed to using hook electrodes which stimulate the nerve outside the epineurium and have large areas of contact. However, the presence of evoked multi-unit activity on the microchannel electrodes did allow an assessment of *overall* device viability which was found to be greater than 50% after five months of implantation, i.e. neural activity could be observed in greater than four of the eight integrated electrodes in each device. This calculation *included* nine nonfunctional electrodes with broken microwire leads. It should also be noted that the electrical stimulation ramp was performed to 1V, which was possibly submaximal to produce a full compound action potential of the entire sciatic nerve. It is therefore possible that some channels were viable but needed greater stimulation levels. The stimulation ramp also allowed the identification of multiple different axon populations within the various microchannels integrated with electrodes, which was expected based on the randomness of axon regeneration.

Overall, using the regenerative microchannel interface presented here, recordings of single and multi unit action potentials could be made that are comparable if not better in some aspects to what has been previously reported with regard to numbers of functional microchannel electrodes [13]. Notably, the fabrication of this interface was accomplished without the need for advanced metal deposition/patterning and insulation techniques for electrode integration. Instead simple off the shelf microwires were integrated and successfully utilized in a chronic setting. Additional work should focus on protecting the microwires from breakage though, as this was the main source of failure.

The amplitudes of the recorded action potentials also fell within ranges previously reported using a variety of peripheral nerve interfaces from LIFE electrodes to other microchannel based interfaces [11,12,39–41]. While these values fell within ranges reported, they were not consistently as large as reported in studies using microchannels [11–13]. There are a few design characteristics of the microchannel interfaces presented in this work that could contribute to the lower signal amplification. First, the microwire electrodes had a recording region that was 0.097 mm^2. This relatively large electrode/recording area would reduce the amplitude of any recorded action potential because the entire electrode surface is equipotential and therefore tends to average out signals. Furthermore, the microchannels have an amplifying effect, based on the ability to constrain the extracellular fluid surrounding an axon and, in theory, increase the amplitude of the recordable extracellular action potential [2]. The large microchannel size chosen to accommodate the 60 μm diameter microwires and the

fact that the walls 'splay out' due to rolling could have reduced this overall amplifying effect (Fig. 9A and B).

Another important point is much of the modeling and *in vitro* work performed to validate this theory used microchannels of either significantly smaller diameters or longer lengths [9]. While smaller diameters and longer lengths might be expected to result in larger action potential amplitudes, based on the results of this study, they may not be suitable for maintaining healthy axons over chronic periods in amputees. In other acute *in vivo* experiments, cut rootlets or portions of nerves were physically placed in microchannels [11,12]. The axons used in these experiments were freshly harvested axons that had not undergone regeneration and are therefore not readily comparable. In a chronic terminal study, single unit action potentials were recorded through a tungsten microelectrode inserted into an implanted microchannel scaffold at the time of recording[13]. However, the electrode was not permanently integrated into nor implanted along with the microchannel scaffold. Thus completely eliminating the foreign body response to the electrode and the deposition of fibrous tissue on the electrode surface which are fundamental factors in chronic interfacing and would reduce recording capabilities. The experimental paradigm of inserting an electrode at the time of recording also provides one the ability to make multiple attempts at 'searching' for the best units and is simply not possible with integrated electrodes. In the present study, microchannel recording capabilities were evaluated using a regenerative nerve model with permanently implanted electrodes and this chronic experimental paradigm in many ways may account for the reduced amplitudes observed.

It should be noted that an additional significantly longer time point, at least one year, is needed to prove conclusively that regenerated axons from an amputated nerve remain healthy and that stable recordings can be made from them. However, based on all the nerve characteristics investigated here, the regenerative microchannel scaffold provides an environment that permits substantial axon growth and maturation within the device over a considerable time period. The regeneration occurred in a spatially orchestrated manner due to the microchannels, which induced spatial segregation into small groups of axons to the benefit of selective interfacing. Growth through the microchannels resulted in a reformation of stereotypical nerve/axon morphologies and tissue compartmentalization that contributed to chronically stable and healthy regeneration through and past the device without complications of irregular nerve regeneration characterizing a neuroma. These findings support the fundamental criteria for a regenerative peripheral nerve interface targeted towards amputees. Finally, based on the electrophysiology data presented here, action potentials can be recorded from regenerated axons in microchannels with permanently integrated electrodes on a chronic timescale. With this the stability and viability of regenerative microchannel interfacing is established, warranting the development of advanced wiring, packaging, and wireless technologies to be utilized with large electrode count microchannel interfaces for chronic continuous behavioral studies and these are ongoing.

5. Conclusions

Overall the results from the current study demonstrated that the microchannel design provides an efficient platform to support regenerating axons and incorporate electronics for interfacing with small groups of axons. The simple fabrication process with biocompatible materials such as PDMS and SU-8 elevates the potential for easy scale up of production of this device. The ease with which one can incorporate microwire electrodes allows a versatile use of this device where advanced insulation and interconnect techniques are not available. The overall flexibility of the fabrication process to adapt and tailor the microchannels to the nerve size has great value in individualized customization of this device. Further, the re-organization, architecture and composition of the regenerating nerve lacking distal reinnervation targets showed numerous parallels to a normal nerve and underscores the potential for *chronic* bidirectional neuronal communication. The demonstrated capability to use microchannel interfaces to record spontaneous, sensory evoked, and electrically evoked single and multi unit action potentials on a chronic scale in the sciatic nerve after implantation for five months further supports this. These properties of the regenerated nerve when coupled with the interfacing capability of microchannels and the lack of adverse effects characteristic of neuroma formation lends this device to be a valuable element in aiding neural prosthetic control for amputees.

Acknowledgments

The authors would like to acknowledge support from the Defense Advanced Research Projects Agency (DARPA) MTO under the auspices of Dr. Jack Judy through the Space and Naval Warfare Systems Center Pacific Grant/Contract No. N66001-11-C-4167, National Science Foundation award CBET 0651716 (RVB), and National Institutes of Health award T32 EB006343. The authors would like to thank Dr. Balakrishna S. Pai for manuscript editing, Jim Schwoebel for support with tissue sectioning, and Eric Gaupp for tremendous support in immunohistochemistry. AS and JTB would also like to thank Dr. Liang Guo for his mentorship and tutelage regarding photolithography and process development.

References

[1] Navarro X, Krueger TB, Lago N, Micera S, Stieglitz T, Dario P. A critical review of interfaces with the peripheral nervous system for the control of neuroprostheses and hybrid bionic systems. J Peripher Nerv Syst 2005;10:229–58.
[2] Fitzgerald JJ, Lacour SP, McMahon SB, Fawcett JW. Microchannels as axonal amplifiers. IEEE Trans Biomed Eng 2008;55:1136–46.
[3] Grill WM, Mortimer JT. Neural and connective tissue response to long-term implantation of multiple contact nerve cuff electrodes. J Biomed Mater Res 2000;50:215–26.
[4] Tyler DJ, Durand DM. Functionally selective peripheral nerve stimulation with a flat interface nerve electrode. IEEE Trans Neural Syst Rehabil Eng 2002;10:294–303.
[5] Branner A, Stein RB, Fernandez E, Aoyagi Y, Normann RA. Long-term stimulation and recording with a penetrating microelectrode array in cat sciatic nerve. IEEE Trans Biomed Eng 2004;51:146–57.
[6] Ramachandran A, Schuettler M, Lago N, Doerge T, Koch KP, Navarro X, et al. Design, in vitro and in vivo assessment of a multi-channel sieve electrode with integrated multiplexer. J Neural Eng 2006;3:114–24.
[7] Lago N, Ceballos D, Rodríguez FJ, Stieglitz T, Navarro X. Long term assessment of axonal regeneration through polyimide regenerative electrodes to interface the peripheral nerve. Biomaterials 2005;26:2021–31.
[8] Hess A, Young JZ. The nodes of Ranvier. Proc R Soc Lond B Biol Sci 1952;140:301–20.
[9] FitzGerald JJ, Lacour SP, McMahon SB, Fawcett JW. Microchannel electrodes for recording and stimulation: in vitro evaluation. IEEE Trans Biomed Eng 2009;56:1524–34.
[10] Rutten WLC. Selective electrical interfaces with the nervous system. Annu Rev Biomed Eng 2002;4:407–52.
[11] Delivopoulos E, Chew DJ, Minev IR, Fawcett JW, Lacour SP. Concurrent recordings of bladder afferents from multiple nerves using a microfabricated PDMS microchannel electrode array. Lab Chip 2012;12:2540–51.
[12] Minev IR, Chew DJ, Delivopoulos E, Fawcett JW, Lacour SP. High sensitivity recording of afferent nerve activity using ultra-compliant microchannel electrodes: an acute in vivo validation. J Neural Eng 2012;9:026005.
[13] FitzGerald JJ, Lago N, Benmerah S, Serra J, Watling CP, Cameron RE, et al. A regenerative microchannel neural interface for recording from and stimulating peripheral axons in vivo. J Neural Eng 2012;9:016010.
[14] Bunge RP, Bunge MB, Eldridge CF. Linkage between axonal ensheathment and basal lamina production by Schwann cells. Annu Rev Neurosci 1986;9:305–28.
[15] Schmidt CE, Leach JB. Neural tissue engineering: strategies for repair and regeneration. Annu Rev Biomed Eng 2003;5:293–347.
[16] Klinge PM, Vafa MA, Brinker T, Brandis A, Walter GF, Stieglitz T, et al. Immunohistochemical characterization of axonal sprouting and reactive

tissue changes after long-term implantation of a polyimide sieve electrode to the transected adult rat sciatic nerve. Biomaterials 2001;22:2333–43.
[17] Lindenlaub T, Sommer C. Partial sciatic nerve transection as a model of neuropathic pain: a qualitative and quantitative neuropathological study. Pain 2000;89:97–106.
[18] Carlton SM, Dougherty PM, Pover CM, Coggeshall RE. Neuroma formation and numbers of axons in a rat model of experimental peripheral neuropathy. Neurosci Lett 1991;131:88–92.
[19] Munger BL, Bennett GJ, Kajander KC. An experimental painful peripheral neuropathy due to nerve constriction. I. Axonal pathology in the sciatic nerve. Exp Neurol 1992;118:204–14.
[20] Coderre TJ, Grimes RW, Melzack R. Deafferentation and chronic pain in animals: an evaluation of evidence suggesting autotomy is related to pain. Pain 1986;26:61–84.
[21] Wall PD, Gutnick M. Ongoing activity in peripheral nerves: the physiology and pharmacology of impulses originating from a neuroma. Exp Neurol 1974;43:580–93.
[22] Fried K, Govrin-Lippmann R, Rosenthal F, Ellisman MH, Devor M. Ultrastructure of afferent axon endings in a neuroma. J Neurocytol 1991;20:682–701.
[23] Devor M, Govrin-Lippmann R, Angelides K. Na+ channel immunolocalization in peripheral mammalian axons and changes following nerve injury and neuroma formation. J Neurosci 1993;13:1976–92.
[24] Breward J, Gentle MJ. Neuroma formation and abnormal afferent nerve discharges after partial beak amputation (beak trimming) in poultry. Experientia 1985;41:1132–4.
[25] Tyner TR, Parks N, Faria S, Simons M, Stapp B, Curtis B, et al. Effects of collagen nerve guide on neuroma formation and neuropathic pain in a rat model. Am J Surg 2007;193:e1–6.
[26] Srinivasan A, Guo L, Bellamkonda RV. Regenerative microchannel electrode array for peripheral nerve interfacing. In: 2011 5th Int. IEEE/EMBS Conf. Neural Eng IEEE; 2011. p. 253–6.
[27] Clements IP, Kim Y, English AW, Lu X, Chung A, Bellamkonda RV. Thin-film enhanced nerve guidance channels for peripheral nerve repair. Biomaterials 2009;30:3834–46.
[28] Mukhatyar V, Pai B, Clements I, Srinivasan A, Huber R, Mehta A, et al. Molecular sequelae of topographically guided peripheral nerve repair. Ann Biomed Eng 2013;42:1436–55.
[29] Fu SY, Gordon T. The cellular and molecular basis of peripheral nerve regeneration. Mol Neurobiol 1997;14:67–116.
[30] Lacour SP, Fitzgerald JJ, Lago N, Tarte E, McMahon S, Fawcett J. Long microchannel electrode arrays: a novel type of regenerative peripheral nerve interface. IEEE Trans Neural Syst Rehabil Eng 2009;17:454–60.
[31] Ceballos D, Valero-Cabré A, Valderrama E, Schüttler M, Stieglitz T, Navarro X. Morphologic and functional evaluation of peripheral nerve fibers regenerated through polyimide sieve electrodes over long-term implantation. J Biomed Mater Res 2002;60:517–28.
[32] Fawcett JW, Keynes RJ. Peripheral nerve regeneration. Annu Rev Neurosci 1990;13:43–60.
[33] Carpenter MB, Jerome S. Human neuroanatomy. 8th ed. Baltimore: Williams & Wilkins; 1983.
[34] Xu Q-G, Forden J, Walsh SK, Gordon T, Midha R. Motoneuron survival after chronic and sequential peripheral nerve injuries in the rat. J Neurosurg 2010;112:890–9.
[35] Furey MJ, Midha R, Xu Q-G, Belkas J, Gordon T. Prolonged target deprivation reduces the capacity of injured motoneurons to regenerate. Neurosurgery 2007;60:723–32.
[36] Fu SY, Gordon T. Contributing factors to poor functional recovery after delayed nerve repair: prolonged axotomy. J Neurosci 1995;15:3876–85.
[37] Ladak A, Schembri P, Olson J, Udina E, Tyreman N, Gordon T. Side-to-side nerve grafts sustain chronically denervated peripheral nerve pathways during axon regeneration and result in improved functional reinnervation. Neurosurgery 2011;68:1654–65. discussion 1665–6.
[38] Bunge RP. The role of the Schwann cell in trophic support and regeneration. J Neurol 1994;242:S19–21.
[39] Branner A, Normann RA. A multielectrode array for intrafascicular recording and stimulation in sciatic nerve of cats. Brain Res Bull 2000;51:293–306.
[40] Dhillon GS, Lawrence SM, Hutchinson DT, Horch KW. Residual function in peripheral nerve stumps of amputees: implications for neural control of artificial limbs. J Hand Surg Am 2004;29:605–15. discussion 616–8.
[41] Rossini PM, Micera S, Benvenuto A, Carpaneto J, Cavallo G, Citi L, et al. Double nerve intraneural interface implant on a human amputee for robotic hand control. Clin Neurophysiol 2010;121:777–83.